**FACTA UNIVERSITATIS**
Series: **Mechanical Engineering** Vol. 23, No 2, 2025, pp. 287 - 310
https://doi.org/10.22190/FUME231221005B

**Original scientific paper**

# NUMERICAL STUDY OF A NON-NEWTONIAN PHASE CHANGE FLOW IN FINNED RECTANGULAR ENCLOSURES

**Mohamed Boujelbene[1], Seyed A.M. Mehryan[2], Mikhail Sheremet[3], Mohammad Shahabadi[4], Nasrin B.M. Elbashir[5], Mohammad Ghalambaz[3]**

[1]Industrial Engineering Department, College of Engineering, University of Ha'il, Ha'il, Saudi Arabia
[2]Young Researchers and Elite Club, Yasooj Branch, Islamic Azad University, Yasooj, Iran
[3]Laboratory on Convective Heat and Mass Transfer, Tomsk State University, Tomsk, Russia
[4]School of Aerospace and Mechanical Engineering, University of Oklahoma, Norman, OK, United States of America
[5]Department of Mathematics, College of Science and Humanities, Prince Sattam Bin Abdulaziz University, Al Kharj, Saudi Arabia

ORCID iDs: Mohamed Boujelbene https://orcid.org/0000-0001-7424-6685
Seyed A.M. Mehryan https://orcid.org/0000-0001-8812-5905
Mikhail Sheremet https://orcid.org/0000-0002-4750-0227
Mohammad Shahabadi https://orcid.org/0000-0003-2753-9519
Nasrin B.M. Elbashir https://orcid.org/0009-0004-6122-403X
Mohammad Ghalambaz https://orcid.org/0000-0003-0965-2358

**Abstract**. *Phase change materials (PCMs) are widely used for thermal energy storage systems due to their effective thermal properties for energy accumulation. Simultaneously, this material has poor thermal conductivity, and for the optimization of such systems, many techniques are used. This study focuses on an analysis of PCMs in a vertical cavity with one, two, or three solid fins and differential heating. The finite element procedure has solved governing equations formulated using the power-law approach for the non-Newtonian PCM and enthalpy-porosity method. The developed code has been verified using numerical and experimental data from other authors. Effects of fins number and power-law index on flow and thermal structures within the cavity have been studied. It has been found that a rise in the power-law index illustrates a growth of time for the charging level of the storage system, while the addition of a solid fin from one to three allows for reducing the charging time. The extended heat transfer surface can be applied to optimize the thermal energy storage system.*

**Key words**: *Non-Newtonian phase change material, Enthalpy-porosity method, Fin-assisted latent heat energy storage, Rectangular enclosures*

Received: December 21, 2023 / Accepted February 15, 2024
**Corresponding authors**: Mohammad Ghalambaz and S.A.M. Mehryan
Laboratory on Convective Heat and Mass Transfer, Tomsk State University, 634050 Tomsk, Russia
E-mail: m.ghalambaz@gmail.com
Young Researchers and Elite Club, Yasooj Branch, Islamic Azad University, Yasooj, Iran,
E-mail: alal171366244@gmail.com

## 1. INTRODUCTION

Phase change materials (PCMs) are widely used for thermal energy storage systems due to their effective thermal properties for energy accumulations. They are important in waste heat recovery systems and sustainable energy [1, 2, 3]. The advantage of PCMs as the most common candidate for a thermal energy storage system is that they store and release a huge quantity of energy at a specific temperature [4, 5]. There are several sectors in which the application of PCMs is considerable, like heating and cooling of buildings [5-7], domestic hot water tanks [9, 10], and solar energy systems [11-13].

One important approach in thermal storage systems is to increase the heat transfer rate and consequently improve their performance [4]. One common way to enhance the melting and solidification time of PCMs in cavities is to use extended fins. They help enhance heat transfer by thinning and breaking down the thermal boundary layer [15]. In this regard, Wu et al. [16] investigated the effects of a fin's length and location on the PCM's phase change in a latent heat thermal energy storage (LHTES). They performed transient numerical simulations employing the enthalpy-porosity method. They reported a considerably shortened time of solidification and melting of PCM with embedded fin. Two geometric parameters of fin length to cavity length (εL) ratio and fin height to cavity height were considered ($\varepsilon_H$). For $\varepsilon_L$ = 0.25, 0.5, and 0.75, the melting time was reduced by 10.4%, 20%, and 26.8%, respectively, and for $\varepsilon_H$ = 0.75, 0.5, and 0.25, the melting time was shortened 9.6%, 20%, and 30.8%, respectively. It was seen that increasing the fin length intensively decreases the solidification time, and lowering the fin position exacerbated the non-uniform distribution of temperature during the solidification process. In another study, Sinaga et al. [17] inspected the effects of the position and shape of two fins on the melting of PCM in a quadrilateral cavity. They chose Lauric acid as the PCM material. They considered three different rectangular, trapezoidal, and triangle shapes for fins and three different heights in the cavity. They discovered that the best melting process happens when the fins are located in the bottom half. In the case of fin shapes, the triangular shape of fins showed the best results and decreased the whole melting time by 1000 seconds. Arshad et al. [18] studied the heat transfer and flow-field characteristics of a heat sink, including PCM and fins. The application of their heat sink was in the passive cooling of electronic devices for input heating powers of 4, 5, and 6 W, and fins of 2mm/3mm thickness occupied 9% volume fraction were employed. They observed a uniform heat distribution in the heatsink, and higher power levels led to a higher melting rate of the PCM. Also, they found out that heat penetration in a 2 mm thick fin was more than the other one, leading to a shorter melting time. Tian et al. [19] examined the influence of fin on the melting of PCM in a rectangular cavity numerically. They evaluated the melting process by six indicators of cost per energy stored, stored energy per mass, mean power, total stored energy, surface averaged Nusselt number, and melting time. Steel302 stored the highest total energy among other materials, and copper fin had the highest mean power. The results showed that the aluminum fin is preferred, while copper is less beneficial than aluminum. Raj et al. [20] investigated the effects of fin thickness, fin shape, the total number of fins, and base thickness on the behavior of a solid-solid PCM thermal management module used in avionics systems for satellites.

The study was done for "on" and "off" cycles of 10W at 1200s and at 4800s, respectively. Their results showed good heat transfer for straight fin configurations with a square shape; however, triangular ones performed better and showed 25% and 35% lower mass compared to circular and square fins for a fixed volume fraction.

Considering different working conditions, a non-linear relation could exist between shear stress and shear rate defined as non-Newtonian fluids. There have been investigations on the thermofluidic characteristics of these fluids. Ohta et al. [21] numerically investigated the natural convection characteristics of a pseudoplastic fluid in a squared cavity. The cavity was heated from the bottom wall. They reported that the heat transmission rate of pseudoplastic fluid is greater than Newtonian fluid due to the easier development of fluid flow, especially close to the walls, by the shear-thinning effects and viscosity reduction. Pandey et al. [22] studied the thermofluidic characteristics of a round cylinder within a square cavity containing non-Newtonian fluid. Their investigations were performed for the Prandtl number 10 and Rayleigh numbers 1E3 to 1E6. The power-low index range of $n = 0.6$ to $n = 1.6$ was considered in their study. At $n = 0.6$, their results showed a steady to unsteady flow transition due to the shear thinning regime. The highest range of Nusselt number was seen for the cylinder case located at the lower part close to the bottom wall. Compared to Newtonian fluid, the heat transfer rate around the cylinder was improved for the cavity occupied by pseudoplastic fluid and decreased for the dilatant one. In another experimental and numerical study, Pandey et al. [23] examined a pseudoplastic fluid's thermal and flow characteristics within a differentially heated square enclosure in three different Rayleigh numbers. They used a new particle image velocimetry approach for the experimental part. They observed good agreement between the numerical and experimental results in the case of magnitude and pattern of velocity at the walls and core of flow. The thermal and hydrodynamic boundary layers were developed close to the side walls quickly. They discovered that there is a directly proportional relationship between the Rayleigh number and the mean Nusselt number. Yang and Du [24] conducted a comprehensive review of the convective heat transfer of nan-Newtonian fluids heated in a cavity. They introduced two main models of power-law and Bingham for formulating non-Newtonian fluids. In the case of non-Newtonian PCMs, Ghalambaz et al. [25] investigated the melting process within a cylindrical cavity between two tubes. They used the finite element method for their numerical calculations. They studied the effects of the Darcy number, non-Newtonian power-low index, and Rayleigh number on the melting of the PCM. They reported a sharp increase in PCM melting by rising Rayleigh to 105 as the conductive heat transmission regime changes to convective. The melting process was enhanced by increasing the Darcy number as the flow circulation increased in the porous area. Mehryan et al. [26] investigated the melting of a power-low non-Newtonian PCM containing nanoparticles in the area between two upright cylinders. The temperature of the inner cylinder was higher than that of the outer cylinder. The method used in this study was the Galerkin finite element method. They reported that the added nanoparticles in PCM reduced melting owing to the rise of the PCM viscosity and the decrease of the average Nusselt number. Farahani et al. [27] numerically inspected the phase change process of non-Newtonian PCM in a double tube and a finned triple tube. They examined the effects of non-Newtonian model parameters, geometrical parameters, and non-uniform magnetic fields on the melting process. They reported an 11-31% increase in the triple-tube configuration compared to the double-tube configuration. Besides, long fins led to good melting by about 19-53% and 30-63% improved mean Nusselt number compared to non-fin case. The increase in the non-Newtonian power low index led to a decrease in the melt fraction and Nusselt number. Mehryan et al. [28] examined the heat transfer rate of nano-enhanced PCM behaving as a non-Newtonian fluid embedded in a porous medium. The solid matrix was made of Aluminum foam, PCM was made of n-octadecane, and nanoparticles of mesoporous

silica ($MPSiO_2$) were chosen for this study. They found out that growth in the concentration of the nanoparticles reduced the normalized molten volume and the average Nusselt number. Also, their results showed that porosity directly affects the phase change phenomena.

Checking the effects of fins in cavities filled with non-Newtonian fluid, Shahabadi et al. [29] studied the thermofluidic characteristics of a power-law non-Newtonian fluid in a cavity. The cavity of their study contains a flexible fin, insulated top and bottom walls, and hot left and low-temperature right walls. They modeled the deformation of the fin by employing the fluid-structure interaction method. Their results showed a significant deflection of a flexible fin of dilatant fluid compared to Newtonian and pseudoplastic fluids. The hot wall's heat transfer decreased as the non-Newtonian power low increased. Anand et al. [30] studied the fluid-solid interaction in a shallow microchannel filling by a non-Newtonian fluid, including a linearly elastic top wall and other rigid walls. They used lubrication theory for the flow problem and two plate theories for the structural problem. They reported an intense reduction of the pressure drop in the microchannel due to the presence of flexible elements.

As seen above, there have been different studies on PCM and heat transfer characteristics of storage systems, including PCMs and/or non-Newtonian fluids. However, there has been no study covering the melting process of non-Newtonian PCM inside a cavity, including fins, to see their effects on the melting process.

## 2. MATHEMATICAL MODEL

The solid-liquid phase change flow of a non-Newtonian PCM is investigated in the present study, as shown in schematic Fig. 1. As depicted, a high temperature ($T_h$) is imposed on the right wall of different configurations of un-finned enclosure and finned rectangular enclosures having 1, 2, and 3 fins. However, the other bounds of the enclosed media are fully insulated. A phase change material with a non-Newtonian power law pattern in the liquid phase is poured within the container. It is worth noting that the volume of fins is known as a constraint. Volume change of the non-Newtonian PCM during the phase transition is insignificant. To capture the effects of the natural convection, the Boussinesq linear approximation was employed.

Considering unsteady, incompressible, laminar, and non-Newtonian conditions for the flow, the continuity, energy, and momentum equations, along with the porosity-enthalpy technique, can be presented as the following [1, 25, 31, 32]:

$$\nabla^* \cdot \vec{u} = 0\,, \tag{1}$$

$$\rho_{PCM}\left[\frac{\partial \vec{u}}{\partial t} + (\vec{u}\cdot\nabla^*)\vec{u}\right] = \nabla^* \cdot \left[-pI + \mu_{PCM}(\nabla^*\vec{u} + (\nabla^*\vec{u})^{tr})\right] + \vec{f}_b + \vec{f}_m\,, \tag{2}$$

where

$$\mu_{PCM}(\dot{\gamma}) = m_{PCM}\dot{\gamma}^{n-1} \;\Bigg|\; \begin{cases} \dot{\gamma} = max\left(\sqrt{[D']:[D']},\ \dot{\gamma}_{min}\right) \\ 2D' = (\nabla\vec{u} + (\nabla\vec{u})^{tr}) \end{cases} \tag{3}$$

$$\vec{f}_b = f_{b,x} i + f_{b,y} j \begin{cases} f_{b,x} = 0 \\ f_{b,y} = (\rho\beta)_{PCM}\, g(T - T_{fu}) \end{cases}, \tag{4}$$

$$\vec{f}_m = f_{m,x} i + f_{m,y} j \begin{cases} f_{m,x} = a_{mush} \dfrac{(1-\Upsilon)^2}{\Upsilon^3 + e} u, \\ f_{m,y} = a_{mush} \dfrac{(1-\Upsilon)^2}{\Upsilon^3 + e} v \end{cases}, \tag{5}$$

$$(\rho C_p)_{PCM} \left[ \frac{\partial T}{\partial t} + \vec{u} \cdot \nabla^* T \right] = \nabla^* \cdot (k_{PCM} \nabla^* T) - (\rho L)_{PCM} \frac{\partial \Upsilon}{\partial t}, \tag{6}$$

$$(\rho C_p)_{sf} \frac{\partial T}{\partial t} = \nabla^* \cdot (k_{sf} \nabla^* T), \tag{7}$$

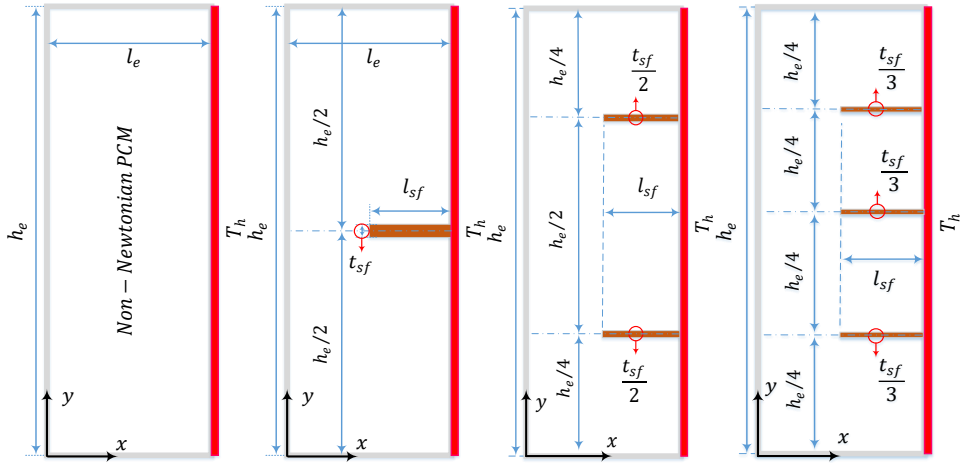


**Fig. 1** Schematic view of the different analyzed configurations

The mathematical form of the applied boundary conditions is:

On the right wall: $$T = T_h,\ u = v = 0 \tag{8}$$

The other walls: $$\frac{\partial T}{\partial N^*} = 0,\ u = v = 0 \tag{9}$$

The computational domain is exposed to the following initial condition:

$$T = T_{initial},\ u = v = 0 \tag{10}$$

On the edge wall of the solid fin and the PCM:

$$-k_{sf} \frac{\partial T}{\partial N^*}\bigg)_{fin} = -k_{PCM} \frac{\partial T}{\partial N^*}\bigg)_{PCM},\ u = v = 0 \tag{11}$$

It is worth noting that $N^*$ in the Eqs. (9) and (11) is the perpendicular direction to the surface.

## 3. THE NORMALIZED CONTROLLING EQUATIONS

Before simulating the correlations, the conversion to non-dimensional coordinates is performed:

$$X=\frac{x}{h_e},\ Y=\frac{y}{h_e},\ U=\frac{uh_e}{\alpha_{PCM}},\ V=\frac{vh_e}{\alpha_{PCM}},\theta=\frac{T-T_{fu}}{T_h-T_{fu}},$$
$$P=\frac{h_e^2 p}{\rho_{PCM}\alpha_{PCM}^2},\ Fo=\frac{t\alpha_{PCM}}{h_e^2},\ \nabla=h_e\nabla^* \tag{12}$$

The equations in non-dimensional form, derived from the aforementioned correlations, can be expressed as:

$$\nabla\cdot\vec{U}=0 \tag{13}$$

$$\frac{\partial\vec{U}}{\partial Fo}+\vec{U}\cdot\nabla\vec{U}=\nabla\cdot\left(-PI+Pr\dot{G}^{n-1}(\nabla\vec{U}+(\nabla\vec{U})^{tr})\right)+\vec{F}_b+\vec{F}_m \tag{14}$$

in which
$$\dot{G}=max\left(\left(\sqrt{[D]:[D]}\right),\ \dot{G}_{min}\right)\ \Big|\ D=\frac{\left((\nabla\vec{U})^{tr}+\nabla\vec{U}\right)}{2} \tag{15}$$

where $\dot{G}_{min}$ is the minimum shear rate used to avoid numerical divergence at points where velocity gradients are close to zero.

$$\vec{F}_b=F_{b,X}i+F_{b,Y}j\ \Big|\ F_{b,X}=0,\ F_{b,Y}=RaPr\theta \tag{16}$$

$$\vec{F}_m=F_{m,x}i+F_{m,y}j\ \Bigg|\ \begin{matrix}F_{m,x}=A_{mush}\dfrac{(1-\Upsilon)^2}{\Upsilon^3+e}U,\\ F_{m,y}=A_{mush}\dfrac{(1-\Upsilon)^2}{\Upsilon^3+e}V\end{matrix} \tag{17}$$

where the Rayleigh (*Ra*) and Prandtl (*Pr*) numbers were introduced as:

$$Pr=\frac{m_{PCM}}{\rho_{PCM}}\frac{\alpha_{PCM}^{n-2}}{h_e^{2n-2}},\ Ra=\frac{\rho_{PCM}g\beta_{PCM}\Delta Th_e^{2n+1}}{m_{PCM}\alpha_{PCM}^n},\ A_{mush}=\frac{a_{mush}h_e^2}{\rho_{PCM}\alpha_{PCM}} \tag{18}$$

The values of $A_{mush}$ and *e* of the above equations are $5\times10^5$ and $10^{-3}$, respectively.

$$\frac{\partial\theta}{\partial Fo}+\vec{U}\cdot\nabla\theta=\nabla^2\theta-\frac{1}{Ste}\frac{\partial\Upsilon}{\partial Fo} \tag{19}$$

Here, the Stefan number (*Ste*) is introduced as:

$$Ste=\frac{C_{p,PCM}\Delta T}{L_{PCM}},\ \Delta T=T_h-T_{fu} \tag{20}$$

$$\frac{(\rho C_p)_{sf}}{(\rho C_p)_{PCM}} \frac{\partial \theta}{\partial Fo} = \frac{k_{sf}}{k_{PCM}} \nabla^2 \theta \tag{21}$$

It is worth noting that the ratios of $(\rho C_p)_{sf} / (\rho C_p)_{PCM}$ and $k_{sf} / k_{PCM}$ are 1.5 and 500, respectively. The thermal and dynamic conditions of the walls in dimensionless format can be expressed as follows, beginning with the condition for the high-temperature boundary:

$$\theta = 1,\ U = V = 0 \tag{22}$$

The other walls:

$$\frac{\partial \theta}{\partial N} = 0,\ U = V = 0 \tag{23}$$

The cavities' initial conditions for velocity and initial temperature are zero:

$$\theta = \theta_{initial},\ U = V = 0 \tag{24}$$

At the edge of the fin -PCM:

$$\frac{k_{sf}}{k_{PCM}} \frac{\partial \theta}{\partial N}\Big)_{fin} = \frac{\partial \theta}{\partial N}\Big)_{PCM},\ U = V = 0 \tag{25}$$

The key parameters of interest are the Nusselt number at the heated surface and the molten fraction. To normalize the melt volume fraction, it is divided by the total volume of the cavity space Thus, MVF is defined as:

$$MVF = \frac{Volume\ of\ the\ melted\ PCM}{Total\ volume\ of\ the\ PCM\ (solid\ and\ liquid)} \tag{26}$$

To evaluate the difference between *MVF* for different values of *n* and *MVF* corresponding to *n* = 1, the following parameter can be defined:

$$P_n = \frac{MVF_n - MVF_{n=1}}{MVF_{n=1}} \tag{27}$$

The heat transfer rates in non-dimensional form for the fluid adjacent to the hot wall and the fin base are given by:

$$Nu_{PCM} = -\frac{\partial \theta}{\partial X}\Big|_{X=0} \tag{28}$$

$$Nu_{sf} = -\frac{k_{sf}}{k_{PCM}} \frac{\partial \theta}{\partial X}\Big|_{X=0} \tag{29}$$

Additionally, the average Nusselt number at the wall is defined as:

$$Nu_{total} = \int_0^{S_1} Nu_{PCM}\, dY + \int_{S_1}^{S_2} Nu_{sf}\, dY + \int_{S_2}^{1} Nu_{PCM}\, dY \tag{30}$$

## 3. NUMERICAL METHOD

The finite element method was applied to solve the equations of mass, momentum, and energy conservation. The initial transformation of the equations into a weak formulation was followed by integration over the physical domain. The solution diagram is shown schematically in Fig. 2. Backward Differential Formulation (BDF) was utilized to govern timesteps to

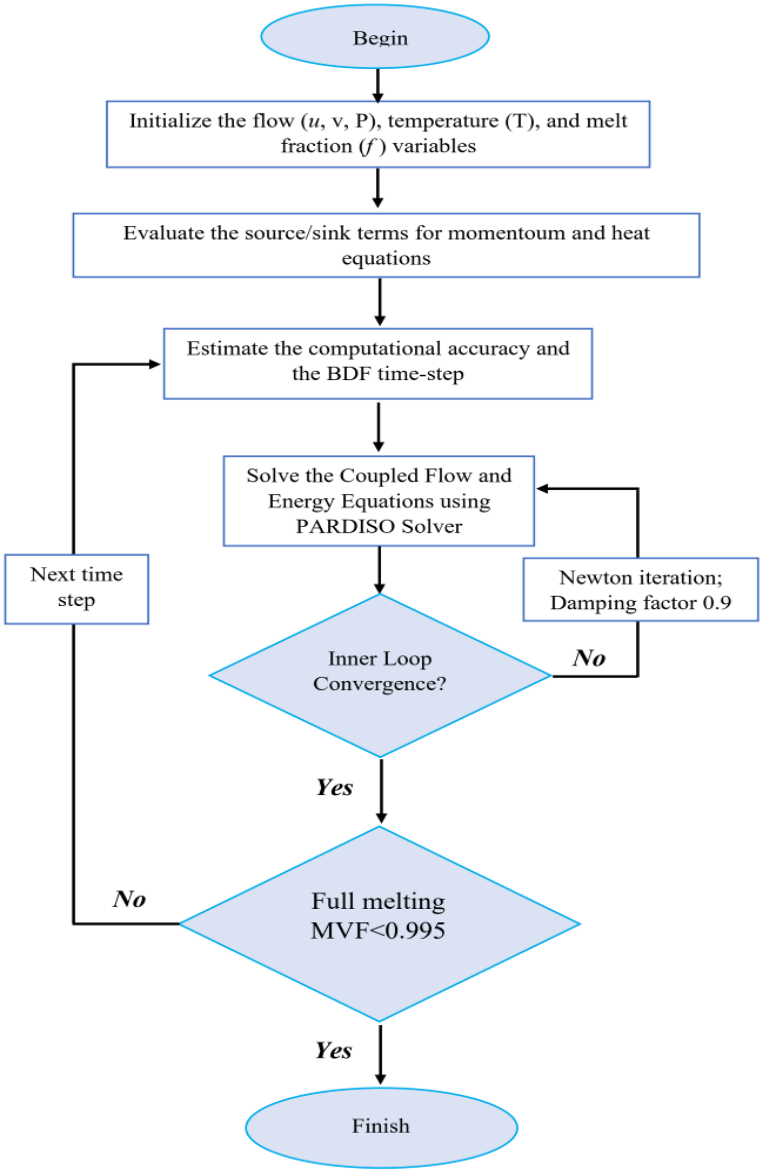


**Fig. 2** Flow chart of the numerical steps

maintain a relative computational accuracy of less than $10^{-4}$. All equations were completely coupled using the Newton technique. [33] provides a full description of the numerical technique. Using the finite element technique in conjunction with the BDF and Newton approach assures the accuracy and dependability of the governing equations' solutions. Fig. 2's solution diagram vividly illustrates the method, emphasizing the integration of the weak formulation over the physical domain. The technique outlined in this section is an integral part of the overall strategy for tackling the issue at hand. The reference to [33, 34] further highlights the rigor and depth of the study's numerical methodology.

## 4. Grid Independency Examination

To discretize the computational domain, triangular elements were chosen. Grid indecency examination is conducted for four grids of 8820 (G1), 24700 (G2), 35880 (G3), and 49420 (G4) elements for $Ra = 1\times105$, $n = 0.6$, $Pr = 1000$. Considering the dependency of the *MVF* on the grid size, the grid with the size of 24700 elements is appropriated to continue the computations. Fig. 3 shows the impact of mesh size on the melting fraction (*MVF*) during the melting process. The utilized mesh for all cases is quite fine to prevent solution instabilities while the time step was controlled by the BDF scheme as discussed in the numerical method. As seen, the variation of mesh sizes has a minimal impact on the solution. Thus, for a fair trade between the computational accuracy and computational cost, the rest of the results were computed using the G2 case.

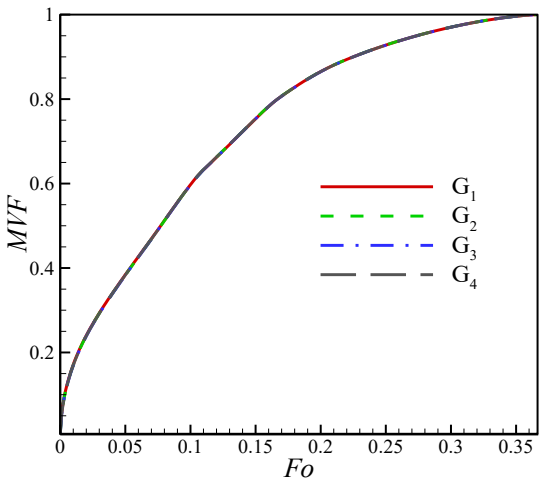


**Fig. 3** The effect of grid size on the melted volume fraction (*MVF*)

## 5. Convergence Analysis

The developed computational code was validated utilizing numerical data from Kebriti and Moqtaderi [35] for the natural convection melting of power-law phase change material in a differentially heated cavity. It is worth mentioning that the dimensionless parameters

in this validation are $Ra = 1.7\times10^5$, $Pr = 1.0$, and $Ste = 0.5$. Fig. 4 shows a very good agreement for the melt flow structure and melting volume for different power-law indexes of the phase change material.

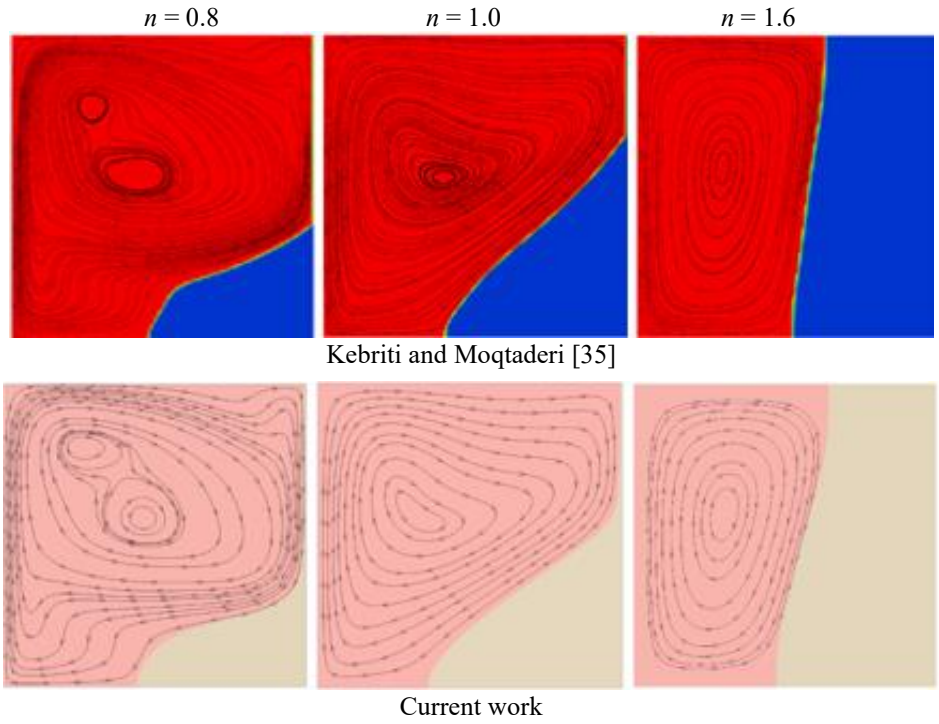


**Fig. 4** Comparison between the obtained results for melting fields and data of Kebriti and Moqtaderi [35]

As another validation, the findings of the present model were compared to those of prior research to verify the simulations' precision and accuracy. This research compares its results to those of Kamkari et al. [36] and Kamkari and Amlashi [37], who studied the melting of lauric acid in an enclosure with a vertical hot wall at a temperature of 70 degrees Celsius. The container was 50 mm in width and 120 mm in height. Fig. 5 displays the findings for two parameters, namely the melting volume fraction (*MVF*) and the local temperature. The comparison demonstrates that the present study's calculations are in reasonable agreement with experimental and numerical literature efforts. This comparison is essential for confirming the accuracy and dependability of the model used in the present research. It offers confidence in the robustness and validity of the simulations by proving that the outcomes are consistent with those of prior research.

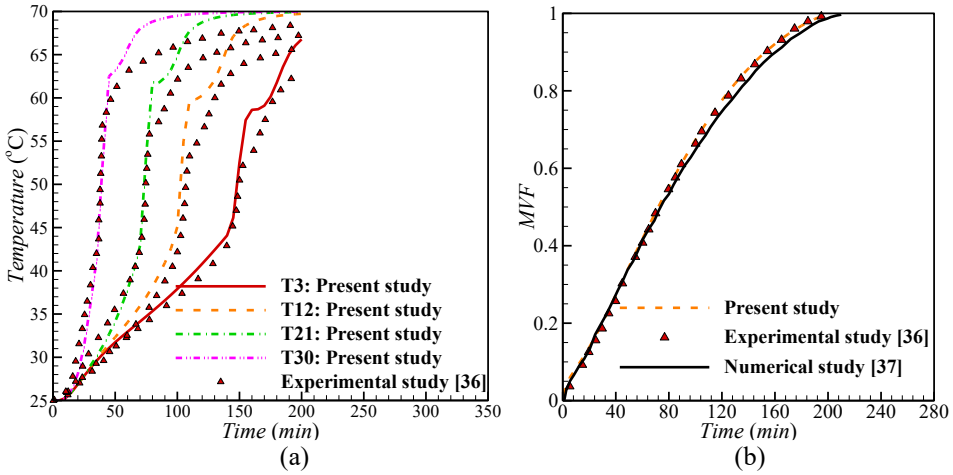


**Fig. 5** Comparison between the results of the current research and those of Kamkari et al. [36] and Kamkari and Amlashi [37]: (a) local temperature and (b) *MVF*

## 6. Results and Discussion

The alterable parameters in this study are non-Newtonian index in the range of 0.6 to 1.4, fins number, and dimensionless time (*Fo*). However, the other parameters, i.e., *Ste*, *Ra*, and *Pr*, are considered fixed in 0.1, $10^5$, and 1000, respectively. Effects of the abovementioned parameters on flow structures and thermal patterns as well as average Nusselt number and melt fraction illustrating the influence of non-Newtonian properties have been scrutinized.

Fig. 6 demonstrates the influence of the power-law index on melting intensity and phase change line location in the case without fins. Thus, regardless of the power-law index value, melting occurs from the right heated wall through the upper cavity part due to an influence of the natural convection mode. More intensive melting occurs for the pseudoplastic liquids when the power-law index is less than 1.0. A reduction of the viscosity with a growth of the shear stress can explain such a nature. As a result, the melting flow becomes more effective with high velocity compared to Newtonian ($n = 1.0$) or dilatant liquids ($n > 1.0$). In the case of dilatant liquids, the liquid viscosity rises with the shear stress. In the case of $n = 0.6$, the whole melting occurs for $Fo = 0.5$, while for $n = 1.0$, melting is not so effective, but in this case, a natural convection regime can also be found. For $n = 1.4$, less obvious distortion of the phase change line can be observed due to attenuation of convective flow and heat transfer with high viscosity with shear stress.

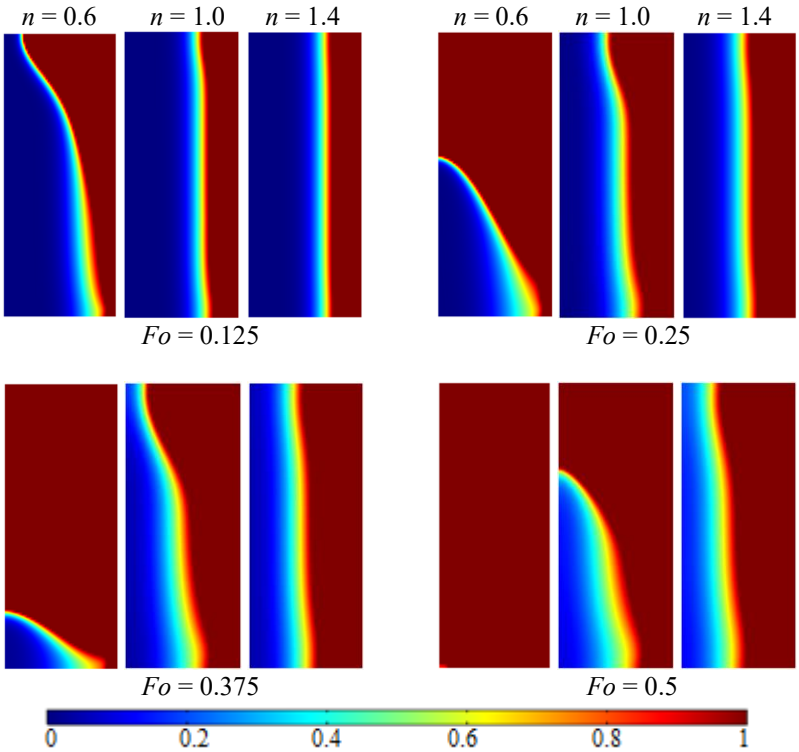


**Fig. 6** Melting contours over time in the cavity without fins for different values of $n$

Fig. 7 presents streamlines and velocity contours for different n with time. This figure can be considered an addition to the previous analysis to scrutinize the flow structure. As mentioned previously, for the pseudoplastic liquid ($n$ = 0.6), more intensive melting occurs, where a counter-clockwise convective cell is formed within the melted part of the region. It is interesting to note that the maximum velocity zone location is displaced from the upper part to the bottom one with time, and these values decrease. Such nature can be explained by a reduction of the temperature difference with time, and as a result, the influence of the buoyancy force becomes less strong than at the beginning of the process. With time, a displacement of the convective cell core to the bottom wall occurs due to the thermal properties of the melt; namely, the Prandtl number of this liquid is high. In the case of Newtonian liquid ($n$ = 1.0), the considered time interval ($0 < Fo \leq 0.5$) is not enough for the whole melting of PCM within the cavity. Still, the structure of the flow cell and maximum velocity zone location is similar to the previous case of dilatant liquid. For dilatant liquid ($n$ = 1.4), it is possible to conclude that the melting occurs due to the heat conduction mode where plane-parallel circulation of the melt can be found.

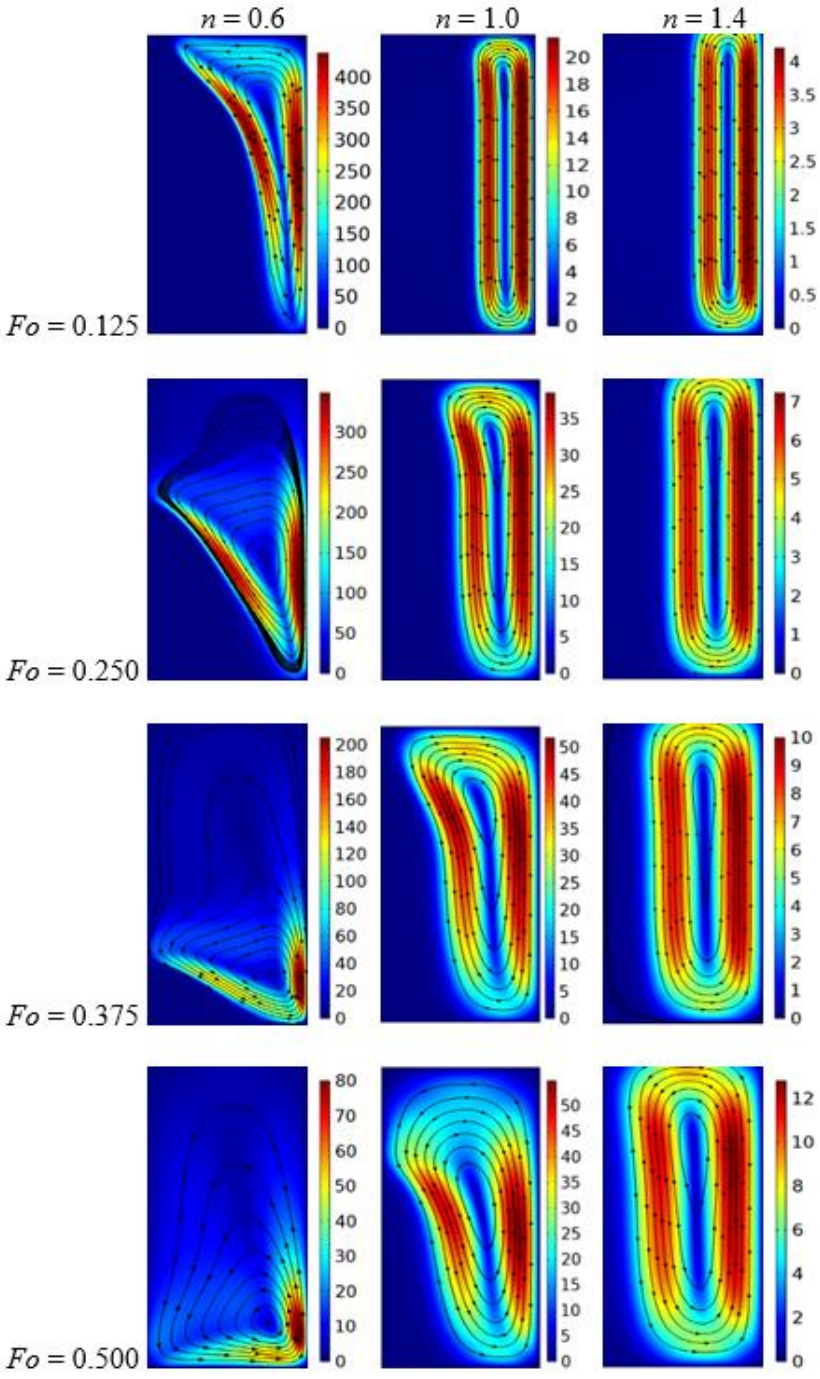


**Fig. 7** Velocity contours and streamlines over time in the cavity without fins for different values of $n$

As mentioned above, a rise in the power-law index characterizes a diminution of the velocity circulation within the chamber. A transition between the considered pseudoplastic liquid and Newtonian liquid characterizes an essential diminution of the circulation velocity compared to the transition between the Newtonian liquid and dilatant liquid.

Figs. 8 and 9 illustrate the flow structures and melt contours within the chamber with one solid fin. The addition of a solid fin characterizes essential melting compared to the case without fins (see Figs. 6 and 7). In the case of pseudoplastic liquid PCM ($n = 0.6$) for $Fo = 0.1$, one can find a formation of complex flow structure near the right heated wall, while for $Fo = 0.2$, the top part of the cavity is wholly melted, and only the lowest part includes the solid phase of PCM. The whole cavity melting occurs up to $Fo = 0.4$. It should be noted that circulation over the solid fin is weak and for $Fo > 0.3$ one can find obvious circulation only under the solid fin. In the case of Newtonian liquid PCM, the melting strength is less compared to that of the pseudoplastic liquid.

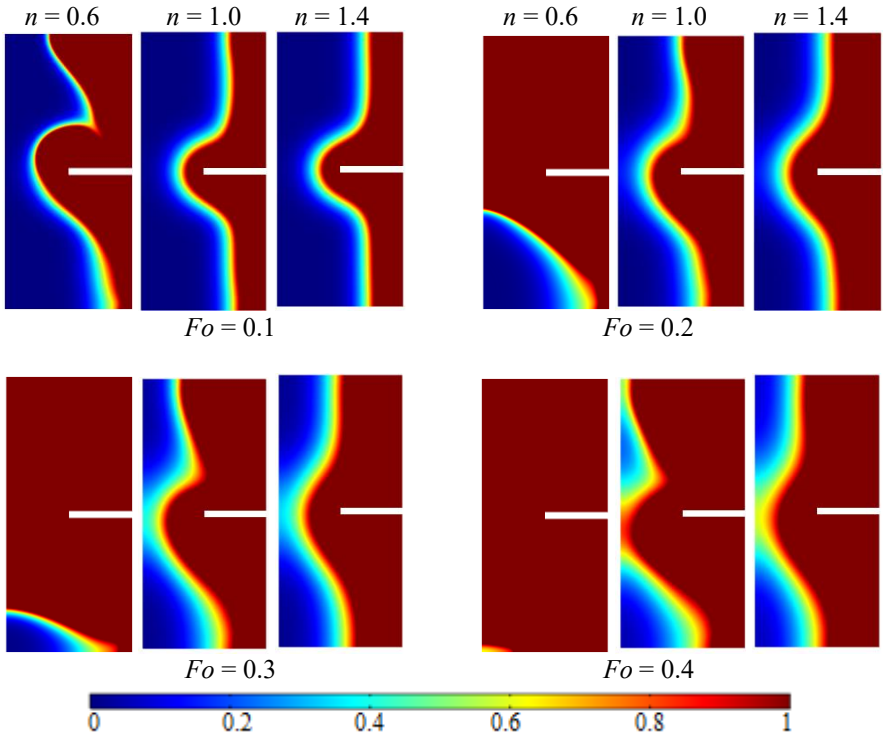


**Fig. 8** A Melting contours over time in the cavity with one fin for different $n$

As shown, the strong circulation can be found only in the upper part of the chamber. Due to more intensive melting of the upper part for $Fo > 0.3$, an asymmetrical flow behavior can be found with intensive circulation in the zone over the solid fin. It should be noted that regardless of the whole melting of the upper part the circulation in this part is strong for $Fo = 0.4$ also. In the case of dilatant liquid PCM ($n = 1.4$) for the considered time interval, symmetrical melting occurs for $0 < Fo < 0.3$, while for $Fo \geq 0.3$ more intensive melting occurs in the upper part with strong circulation in this part.

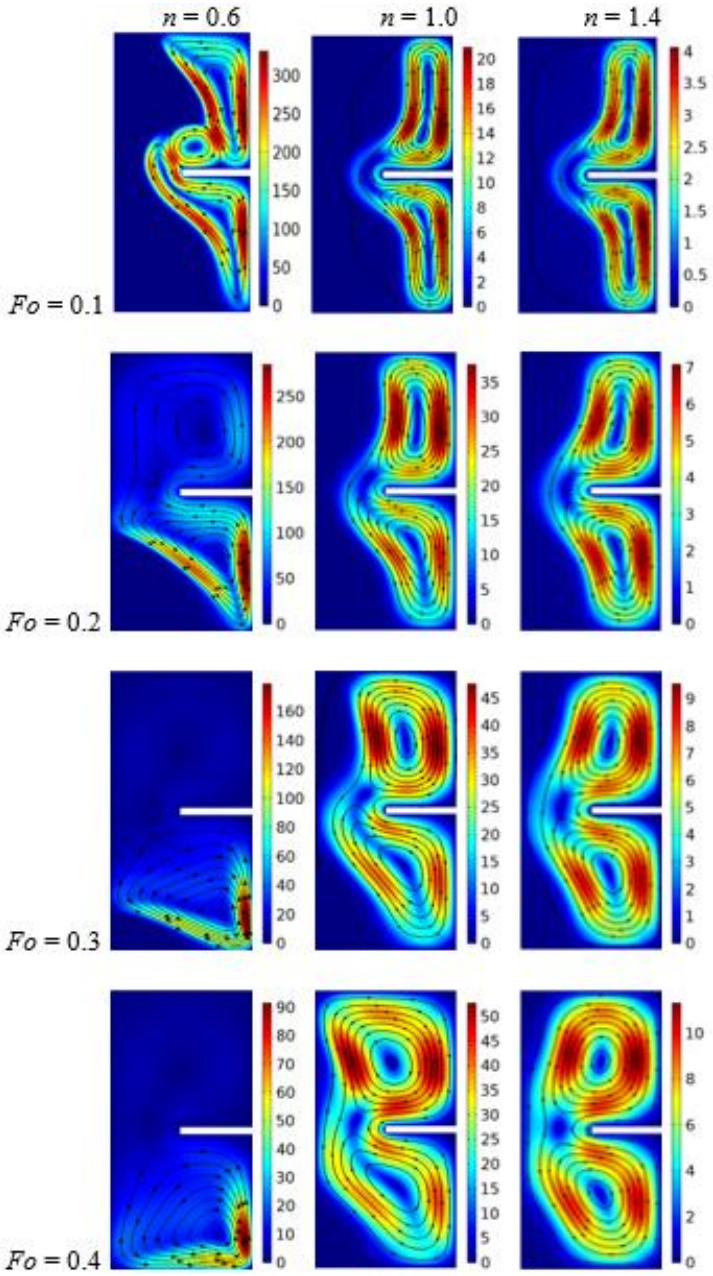


**Fig. 9** Velocity and streamlines contours over time in the cavity with one fin for different values of $n$

As mentioned for the case without a fin, the convective mode is weak for dilatant liquids and it is suppressed with the power-law index. It is necessary to highlight that a transition between the considered pseudoplastic liquid and Newtonian liquid characterizes more essential diminution of the circulation velocity compared to the transition between the Newtonian liquid and dilatant liquid for initial timer level ($Fo < 0.3$), while for $Fo \geq 0.3$ the opposite nature can be found.

An influence of two solid fins on flow structures and melt contours is shown in Figs. 10 and 11. An addition of the second fin allows intensifying the melting process and the charging level accelerates. The case of pseudoplastic liquid PCM characterizes strong melting and the time of $Fo = 0.36$ reflects the whole melting within the chamber.

It is interesting to note that the pseudoplastic liquid reflects an intensive circulation in the bottom part, while for other cases ($n$ =1.0 and $n$=1.4) such strong circulation occurs in the middle and upper zones. A huge reduction of flow intensity occurs with a rise of the power-law index for dilatant fluid, where viscosity increases with the shear stress.

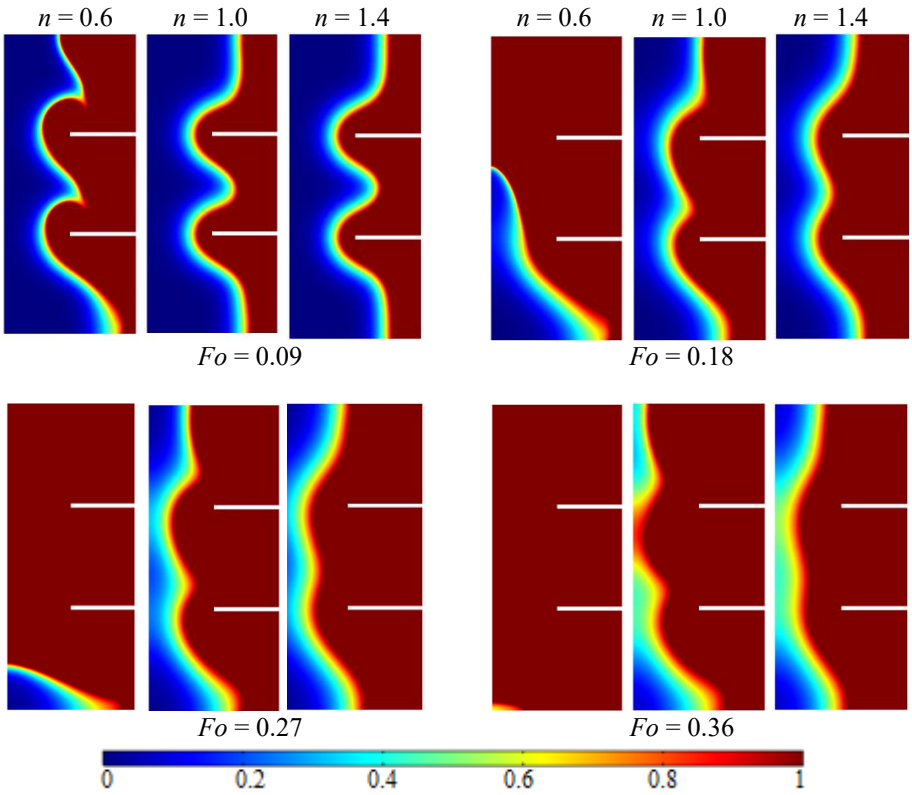


**Fig. 10** Melting contours over time in the cavity with two fins for different values of $n$

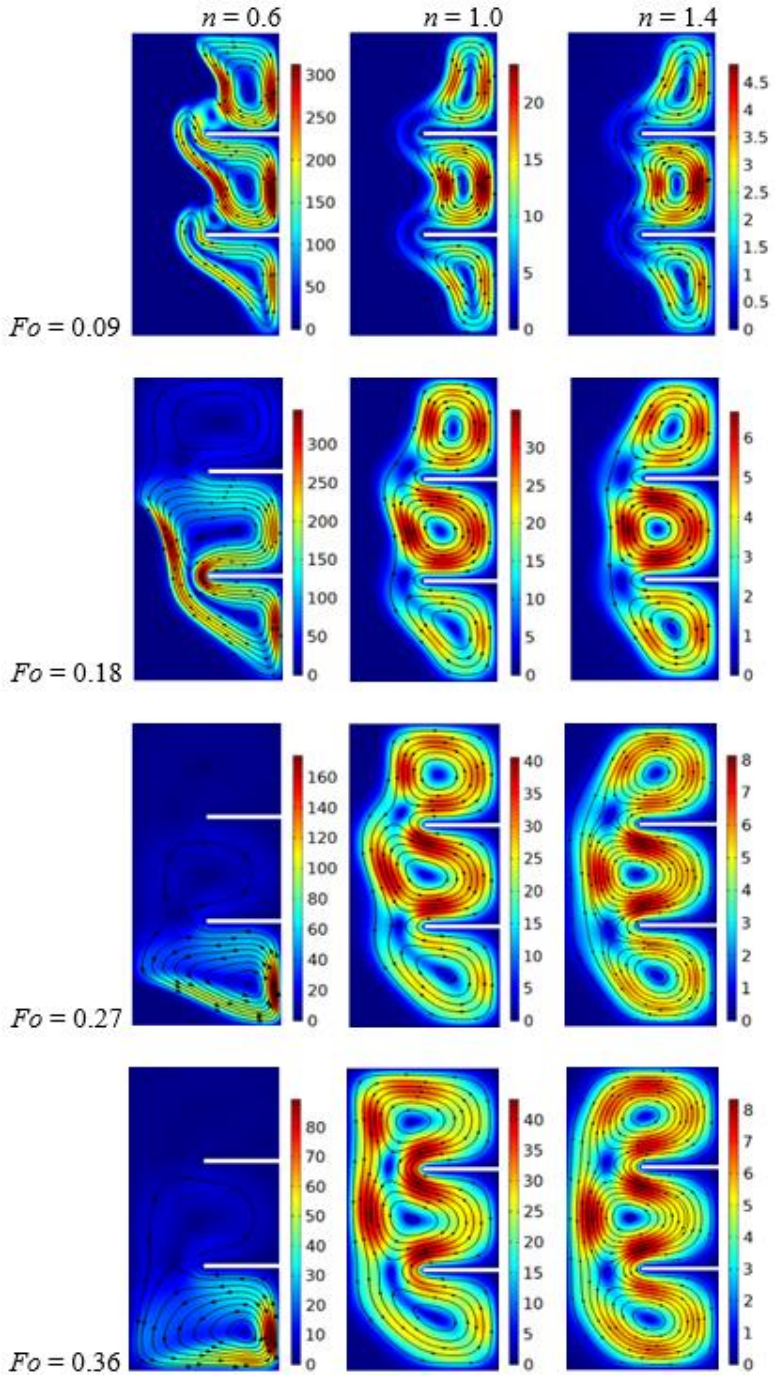


**Fig. 11** Velocity contours and streamlines over time in the cavity with two fins for different values of $n$

The appearance of an additional solid fin illustrates a formation of additional recirculation between fins. In the case of $n = 0.6$ with melting the maximum velocity zone is displaced to the bottom part, while for other cases ($n = 1.0$ and $n = 1.4$) these zones are placed in the middle and upper part and $Fo = 0.36$ is not enough for the whole melting of PCM within the energy storage system. Taking into account these melting contours, the strong melting occurs in the central part where the extended heat transfer surface allows intensifying the thermal dissipation from the heated wall.

Figs. 12 and 13 demonstrate melting and velocity contours in the case of three solid fins. These distributions are similar to the previously studied ones. As a result, adding the third fin characterizes more intensive melting of PCM and a formation of additional recirculation between the solid fins. Melting is more essential in the central part where solid fins are located, and huge heat dissipation can be found from the heated wall. Moreover, comparing these considered cases for different numbers of fins, it is possible to conclude that the growth of the fins' number not only characterizes more essential melting of PCM but also accelerates flow in the convective mode due to flow zone narrowing. It is interesting to emphasize that in the case of pseudoplastic liquid, the velocity circulation decreases with time. In contrast, for other liquids (Newtonian and dilatant), one can find an opposite behavior.

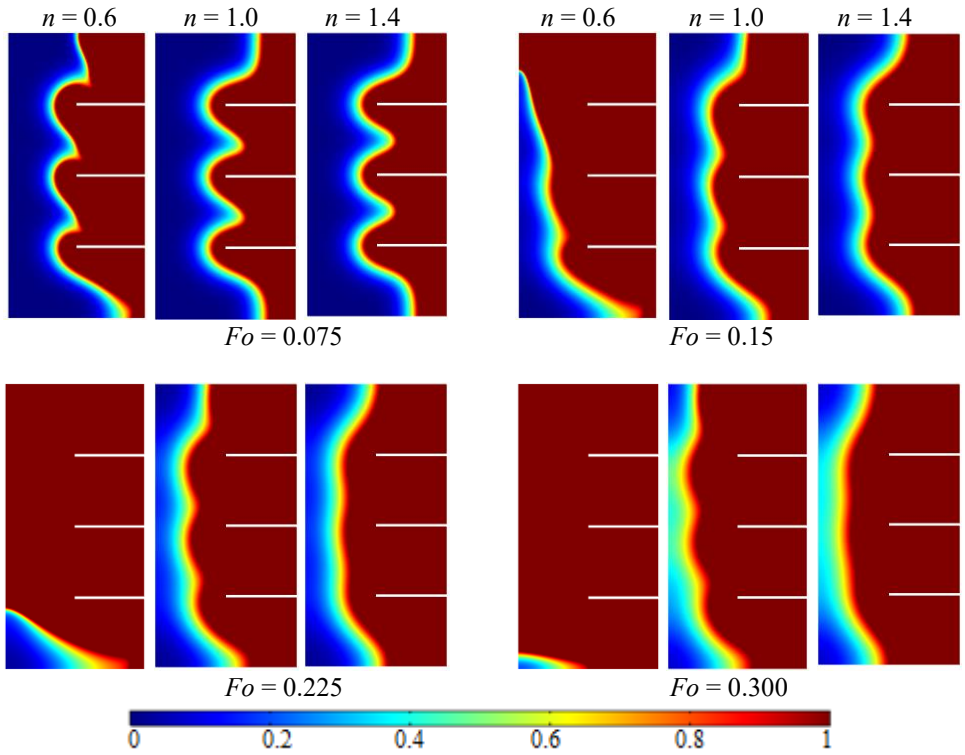


**Fig. 12** Melting contours over time in the cavity with three fins for different values of $n$

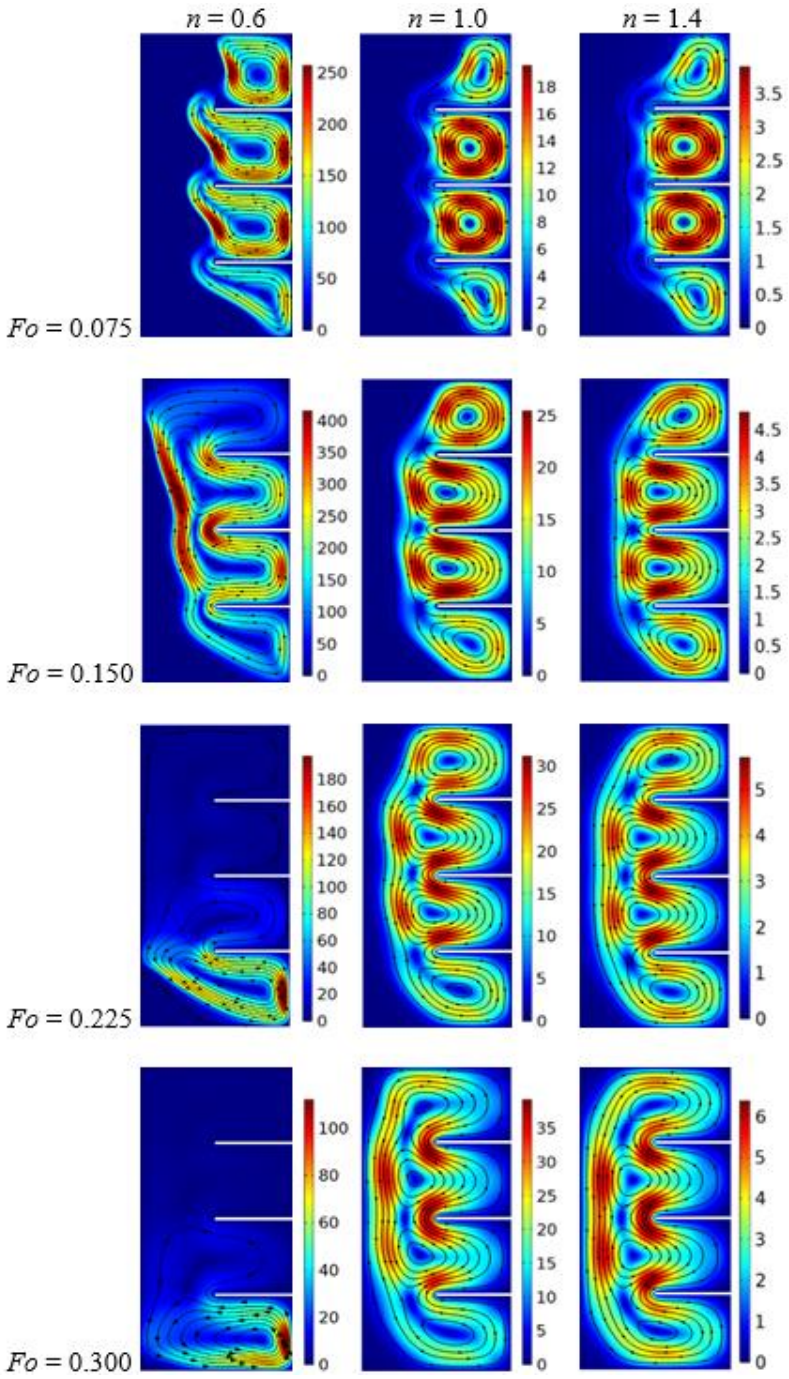


**Fig. 13** Velocity contours and streamlines over time in the cavity with three fins for different values of $n$

Fig. 14 illustrates the time evolution of the melt volume fraction for different numbers of fins and various power-law indexes. Regardless of the number of fins, a rise of the power-law index leads to a growth of time of the whole melting of PCM within the chamber. As mentioned above, more intense melting occurs for the pseudoplastic liquid. An installation of solid fins at the heated wall leads to a decrease in the time of full melting of PCM. Regardless of the solid fins number, the heat conduction level when non-Newtonian liquid does not affect the time behavior of the melt volume fraction can be found for the time interval $0 \le Fo \le 0.05$. While an addition of solid fins characterizes a growth of *MVF* during this heat conduction level. In the case of pseudoplastic liquid, a growth of n between 0.6 and 0.8 reflects an essential rise of the time of whole PCM melting, while for the dilatant liquid, a rise of the power-law index between 1.2 and 1.4 has a weak difference in this time of whole melting. Moreover, an increment of n illustrates a reduction of time difference for the whole PCM melting between Newtonian liquid and considered dilatant liquids. At the same time, the time differences for the pseudoplastic liquids are significant.

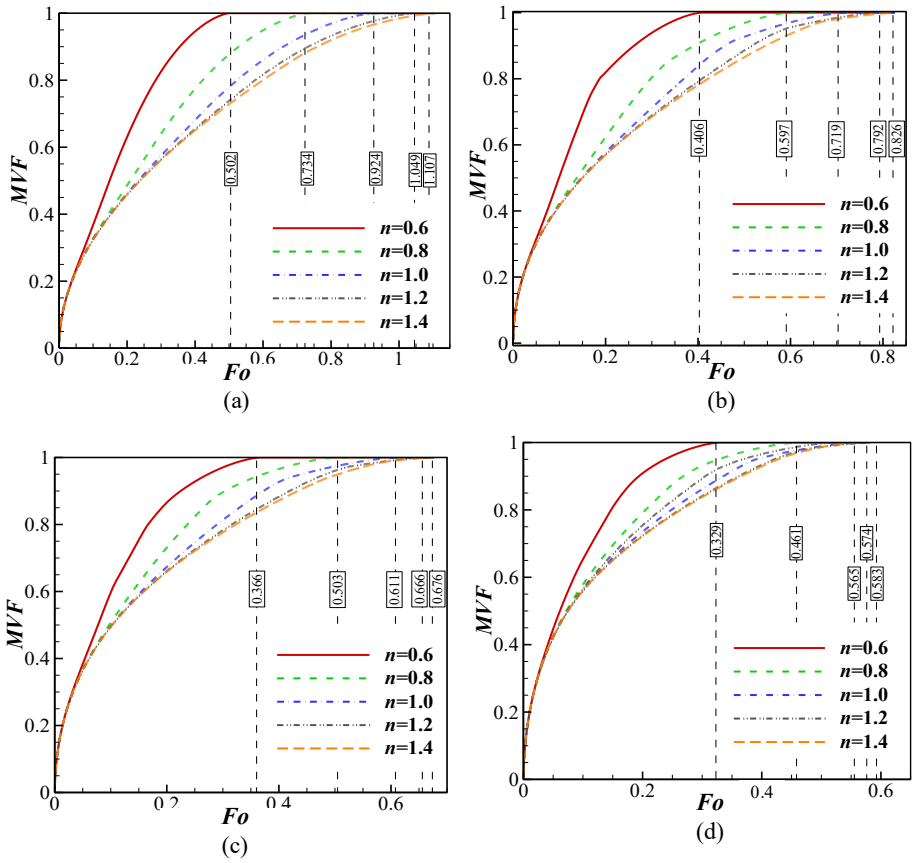


**Fig. 14** Normalized melted liquid fraction for the cavity: (a) without fins, (b) with one fin, (c) with two fins, and (d) with three fins different

Fig. 15 shows the time evolution of $P_n$ with $n$ for different numbers of solid fins. It should be noted that $P_n$ illustrates a relative difference in *MVF* between the current liquid and Newtonian fluid. Taking into account Fig. 15, one can confirm the conclusion mentioned in the previous Fig. 12, namely, an essential difference in *MVF* can be found between pseudoplastic liquid and Newtonian liquid. At the same time, an inclusion of solid fins reduces differences between Newtonian liquid and other PCM liquids.

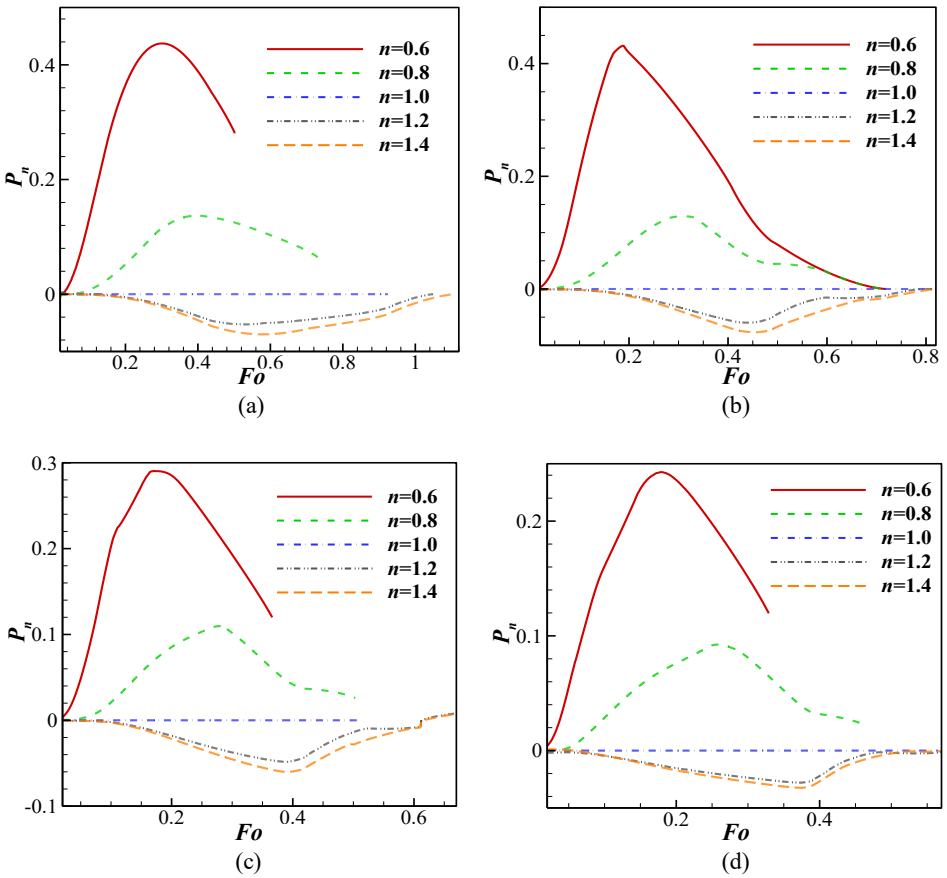


**Fig. 15** Dependency of Pn parameter on the power-law index $n$ for the cavity: (a) without fins, (b) with one fin, (c) with two fins, and (d) with three fins

Evolution of the average Nusselt number at the heated wall with time, power-law index, and solid fins number is demonstrated in Fig. 16. A reduction of the average Nusselt number with time characterizes a diminution of the temperature gradient close to this wall due to heating of the surrounding fluid. The average Nusselt number for dilatant liquids has a weak difference, while this difference is essential for pseudoplastic liquids. Moreover, adding solid fins characterizes a rise in the average Nusselt number. An achievement of zero value illustrates a whole melting of PCM.

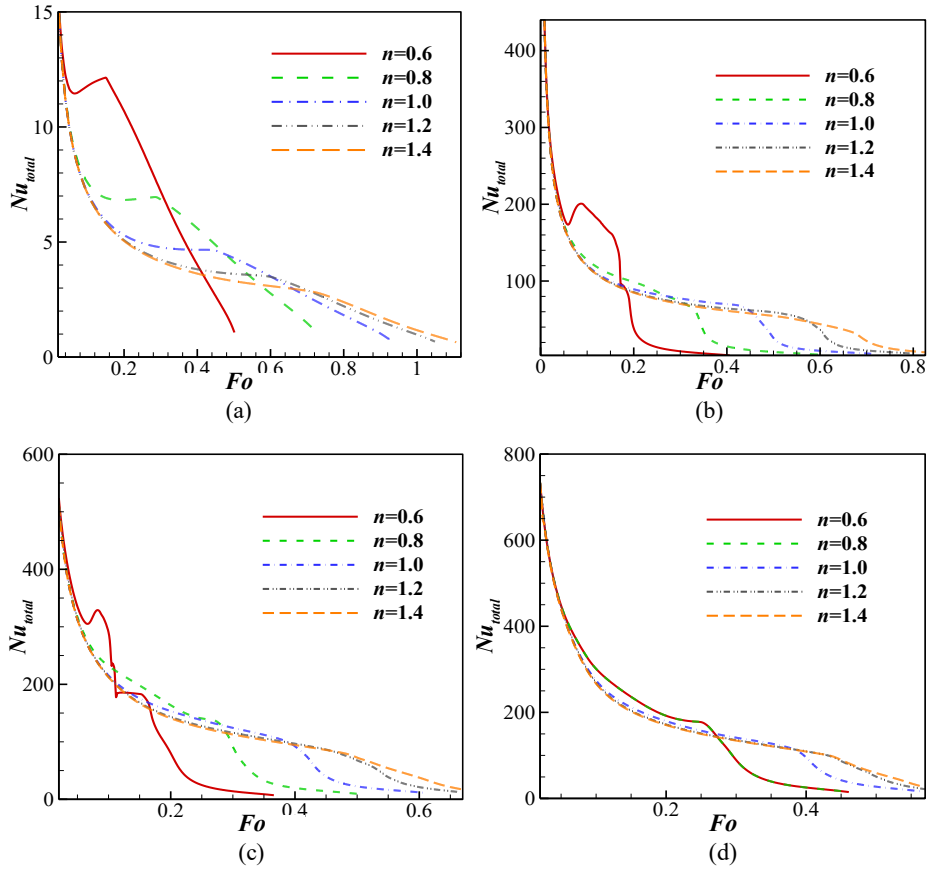


**Fig. 16** Dependency of $Nu_{total}$ on n for the cavity: (a) without fins, (b) with one fin, (c) with two fins, and (d) with three fins

## 7. CONCLUSIONS

Numerical analysis of non-Newtonian PCM convective melting in a differentially-heated cavity with solid fins has been performed. Governing equations formulated using the power-law approach for non-Newtonian liquid, Boussinesq approximation for buoyancy force, and enthalpy-porosity approach for description of the melting process have been solved numerically by the finite element technique. The developed computational code has been validated using the literature numerical and experimental outcomes. Effects of the power-law index, solid fins number, and time on the flow structures and melting patterns have been scrutinized. It has been found that:

- Strong melting of PCM occurs for pseudoplastic fluids ($n < 1$) where the melting time is minimum compared to Newtonian and dilatant fluids.
- A growth of the power-law index characterizes a rise of the melting time for PCM within the considered thermal energy storage system.

- An increment of *n* for dilatant liquids does not have essential differences in melting time and average Nusselt number.
- An addition of solid fins results in a reduction of the melting time and intensification of the phase change process. The melting zone is placed near the thermal dissipation zone, namely, close to the fins' location.
- An increment of the power-law index reflects a diminution of the velocity circulation within the storage system.
- A rise of the fins number characterizes not only more essential melting of PCM, but also flow accelerates in the convective mode due to flow zone narrowing. It is interesting to emphasize that in the case of pseudoplastic liquid the velocity circulation decreases with time, while for other liquids (Newtonian and dilatant) one can find an opposite behavior.

**Acknowledgments**: *This study is supported via funding from Prince Sattam bin Abdulaziz University project number (PSAU/2024/R/1445). This research of Mohammad Ghalambaz and Mikhail Sheremet was supported by the Tomsk State University Development Programme (Priority-2030)..*

## REFERENCES

1. Yan, P., Fan, W., Yang, Y., Ding, H., Arshad, A., Wen, C., 2022, *Performance enhancement of phase change materials in triplex-tube latent heat energy storage system using novel fin configurations*, Applied Energy, 327, 120064.
2. Ghalambaz, M., Jin, H., Bagheri, A., Younis, O., Wen, D., 2022, *Convective Flow and Heat Transfer of Nano-Encapsulated Phase Change Material (NEPCM) Dispersions along a Vertical Surface*, Facta Universitatis, Series: Mechanical Engineering, 20(3), pp. 519-538
3. Saedpanah, E., Lahonian, M., Zare Malek Abad, M., 2023, *Optimization of multi-source renewable energy air conditioning systems using a combination of transient simulation, response surface method, and 3E lifespan analysis*, Energy, 272, 127200
4. Shahabadi, M., Alshuraiaan, B., Abidi, A., Younis, O., Ghalambaz, M., Mehryan, S.A.M., 2022, *Transient melting flow of a NePCM comprising GNPs in a semi-elliptical latent heat thermal energy storage unit*, International Communications in Heat and Mass Transfer, 130, 105815.
5. Farzaneh, F., Jung, S., 2023, *Experimental and numerical investigation on enhancing capped-end tube energy absorption capacity by orifice effect*, Structures, 53, pp. 1450-1462.
6. Al-Yasiri, Q., Szabó, M., 2021, *Influential aspects on melting and solidification of PCM energy storage containers in building envelope applications*, International Journal of Green Energy, 18(9), pp. 966-986.
7. Cunha, S.R.L., Aguiar, J.L.B., 2019, *Phase change materials and energy efficiency of buildings: A review of knowledge*, Journal of Energy Storage, 27, 101083.
8. Castell, A., Martorell, I., Medrano, M., Pérez, G., Cabeza, L.F., 2010, *Experimental study of using PCM in brick constructive solutions for passive cooling*, Energy and buildings, 42(4), pp. 534-540.
9. Cabeza, L.F., Ibanez, M., Sole, C., Roca, J., Nogues, M., 2006, *Experimentation with a water tank including a PCM module*, Solar Energy Materials and Solar Cells, 90(9), pp. 1273-1282.
10. Gracia, A.D., Oró, E., Farid, M., Cabeza, L., 2011, *Thermal analysis of including phase change material in a domestic hot water cylinder*, Applied Thermal Engineering, 31(17-18), pp. 3938-3945.
11. Javadi, F., Metselaar, H., Ganesan, P., 2020, *Performance improvement of solar thermal systems integrated with phase change materials (PCM), a review*, Solar Energy, 206, pp. 330-352.
12. Elashmawy, M., Alhadri, M., Ahmed, M.M., 2021, *Enhancing tubular solar still performance using novel PCM-tubes*, Desalination, 500, 114880.
13. Farid, M.M., Khalaf, A.N., 1994, *Performance of direct contact latent heat storage units with two hydrated salts*, Solar Energy, 52(2), pp. 179-189.
14. Chaturvedi, R., Islam, A., Sharma, K., 2021, *A review on the applications of PCM in thermal storage of solar energy*, Materials Today: Proceedings, 43, pp. 293-297.
15. Webb, R.L., Kim, N., 2005, Enhanced heat transfer, Taylor and Francis, NY.

16. Wu, J., Chen, Q., Zhang, Y., Sun, K., 2021, *Phase change material heat transfer enhancement in latent heat thermal energy storage unit with single fin: Comprehensive effect of position and length*, Journal of Energy Storage, 42, 103101.
17. Sinaga, N., Moria, H., Nisar, K.S., Vu, C.M., Heidarshenas, B., Arsalanloo, A., Youshanlouei, M.M., 2021, *Melting performance enhancement of thermal storage system by utilizing shape and position of double fin*, Case Studies in Thermal Engineering, 23, 100813.
18. Arshad, A., Jabbal, M., Sardari, P.T., Bashir, M.A., Faraji, H., Yan, Y., 2020, *Transient simulation of finned heat sinks embedded with PCM for electronics cooling*, Thermal Science and Engineering Progress, 18, 100520.
19. Tian, L.L., Liu, X., Chen, S., Shen, Z.G., 2019, *Effect of fin material on PCM melting in a rectangular enclosure*, Applied Thermal Engineering, 167, 114764.
20. Raj, C.R., Suresh, S., Bhavsar, R.R., Singh, V.K., Govind, K.A., 2020, *Influence of fin configurations in the heat transfer effectiveness of Solid solid PCM based thermal control module for satellite avionics*: *Numerical simulations*, Journal of Energy Storage, 29, 101332.
21. Ohta, M., Ohta, M., Akiyoshi, M., Obata, E., 2002, *A numerical study on natural convective heat transfer of pseudoplastic fluid in a square cavity*, Numerical Heat Transfer, Part A: Applications, 41(4), pp. 357-372.
22. Pandey, S., Park, Y.G., Ha, M.Y., 2020, *Unsteady analysis of natural convection in a square enclosure filled with non-Newtonian fluid containing an internal cylinder*, Numerical Heat Transfer, Part B: Fundamentals, 77(1), pp. 1-21.
23. Pandey, S., Yoon, S.Y., Balachandar, S., Ha, M.Y., 2022, *Experimental and numerical investigations of thermal and flow characteristics of a shear-thinning non-Newtonian fluid in a differentially heated cavity*, International Journal of Heat and Mass Transfer, 187, 122570.
24. Yang, L., Du, K., 2020, *A comprehensive review on the natural, forced, and mixed convection of non-Newtonian fluids* (*nanofluids*) *inside different cavities*, Journal of Thermal Analysis and Calorimetry, 140(5), pp. 2033-2054.
25. Ghalambaz, M., Ayoubloo, K.A., Hajjar, A., 2020, *Melting heat transfer of a non-Newtonian phase change material in a cylindrical vertical-cavity partially filled porous media*, International Journal of Numerical Methods for Heat & Fluid Flow, 30(7), pp. 3765-3789.
26. Mehryan, S.A.M., Vaezi, M., Sheremet, M., Ghalambaz, M., 2020, *Melting heat transfer of power-law non-Newtonian phase change nano-enhanced n-octadecane-mesoporous silica* ($MPSiO_2$), International Journal of Heat and Mass Transfer, 151, 119385.
27. Farahani, S.D., Farahani, A.D., Tayebzadeh, F., Mosavi, A.H., 2021, *Melting of non-Newtonian phase change material in a finned triple-tube: Efficacy of non-uniform magnetic field*, Case Studies in Thermal Engineering, 28, 101543.
28. Mehryan, S.A.M., Ghalambaz, M., Vaezi, M., Zadeh, S.M.H., Sedaghatizadeh, N., Younis, O., Chamkha, A.J., Abulkhair, H., 2021, *Non-Newtonian phase change study of nano-enhanced n-octadecane comprising mesoporous silica in a porous medium*, Applied Mathematical Modelling, 97, pp. 463-482.
29. Shahabadi, M., Mehryan, S.A.M., Ghalambaz, M., Ismael, M., 2021, *Controlling the natural convection of a non-Newtonian fluid using a flexible fin*, Applied Mathematical Modelling, 92, pp. 669-686.
30. Anand, V., David, J., Christov, I.C., 2019, *Non-Newtonian fluid–structure interactions: Static response of a microchannel due to internal flow of a power-law fluid*, Journal of Non-Newtonian Fluid Mechanics, 264, pp. 62-72.
31. Zhu, Z., Nadimi, E., Asadollahzadeh, M., Bahari, M., Zare Malek Abad, M., Aliehyaei, M., 2023, *Investigation into the effect of multiple line dipoles magnetic field through LS-3 parabolic trough solar system*, Applied Thermal Engineering, 235, 121332.
32. Saghafian, M., Seyedzadeh, H., Moradmand, A., 2023, *Numerical simulation of electroosmotic flow in a rectangular microchannel with use of magnetic and electric fields*, Scientia Iranica.
33. Zienkiewicz, O.C., Taylor, R.L., Nithiarasu, P., 2013, The finite element method for fluid dynamics, Butterworth-Heinemann.
34. Lewis, R.W., Nithiarasu, P., Seetharamu, K.N., 2004, *Fundamentals of the finite element method for heat and fluid flow*, John Wiley & Sons.
35. Kebriti, S., Moqtaderi, H., 2021, *Numerical simulation of convective non-Newtonian power-law solid-liquid phase change using the lattice Boltzmann method*, International Journal of Thermal Sciences, 159, 106574.
36. Kamkari, B., Shokouhmand, H., Bruno, F., 2014, *Experimental investigation of the effect of inclination angle on convection-driven melting of phase change material in a rectangular enclosure*, International Journal of Heat and Mass Transfer, 72, pp. 186-200.
37. Kamkari, B., Amlashi, H.J., 2017, *Numerical simulation and experimental verification of constrained melting of phase change material in inclined rectangular enclosures*, International Communications in Heat and Mass Transfer, 88, pp. 211-219.